A Real-time Pedestrian Dead Reckoning System with FM-Aided Motion Mode Recognition

Haidong Wang, Li Cong, and Honglei Qin

***Abstract*— Accurate indoor pedestrian positioning has attracted extensive research attention along with the rising popularity of indoor location-based service. Among the indoor positioning methods, pedestrian dead reckoning stands out for requiring neither expensive infrastructure nor laborious site survey. However, with time going on, the pedestrian dead reckoning method suffers from error accumulation problem, whereas the major cause of positioning error is usually heading deviation. To tackle the error-drifting problem, a real-time indoor pedestrian dead reckoning system using inertial sensors and frequency-modulated radio receiver is designed in this paper. First a random forest classifier combining frequency-modulated radio signal and inertial sensor signal is devised to achieve real-time identification of straight-line and turning mode of moving. Based on the classification result, constraint is applied to headings in straight periods and true headings are extracted from accelerometer and magnetometer measurements to reduce heading deviation in straight periods. Field experiments have been conducted at three sites in two office buildings to evaluate the performance of the proposed system. Experiment results indicate error drifting can be effectively constrained by the proposed PDR system.**

***Index Terms*— indoor positioning; pedestrian dead reckoning; microelectromechanical sensor; frequency modulation; pattern recognition;**

I. INTRODUCTION

GREAT application potential lies in indoor location-based service (LBS) for its integration of precise positioning and related service. With the aid of indoor LBS, people are able to quickly determine their position and find the optimal route for their target location in large venues like supermarkets and museums. In outdoor regions, Global Navigation Satellite System (GNSS) has been the de facto standard positioning approach after decades of development. However, myriad walls, doors, furniture, together with frequent human activity, cause GNSS signal to suffer from severe attenuation and multipath in indoor environment, resulting in its failure of normal functioning. Consequently, indoor positioning systems have to rely on other methods to provide user location. Indoor positioning systems can be categorized by technique into four major types as concluded by [1]: lateration/angulation systems, proximity systems, radio fingerprinting systems and dead reckoning systems. Lateration/angulation systems work out user location by applying trilateration or triangulation method with measurements of distance or angle between user and base stations [2,3,4,5]. High accuracy might such systems achieve, expensive devices need to be deployed. Systems based on proximity find location of users when they are in the vicinity of pre-deployed tags [6,7]. Although easy to use, it costs both money and time to deploy enough quantities of tags. Another commonly used approach is the indoor fingerprint positioning, which has attracted much attention [8,9,10,11,12] in the past years with its high accuracy. However, the construction of fingerprint database requires laborious and time-consuming site-survey by professional users. Unlike these three kinds of positioning systems, dead reckoning systems [13,14,15,16,17,18] can be readily put into use while neither site-survey nor deployment cost is required.

Dead reckoning systems can be classified into two categories: inertial navigation system (INS) and pedestrian dead reckoning (PDR). The INS approach provides user position by integrating acceleration in the navigation frame whereas the PDR approach adds up displacement vector of each step to locate users. Owing to the double integration in INS, quickly accumulated error could result in tremendous position drift for systems using sensors manufactured with microelectromechanical systems (MEMS) technology. Therefore, to restrict error drifting, practical INS-based pedestrian positioning systems have to fix sensor units to the feet of users and apply specialized constraints like zero velocity update and zero angular rate update [1,15,19]. On the other hand, such requirement about sensor attachment is not compulsory for PDR systems, where sensors can be placed in various places like hand, pocket and bag. Three parts are needed for PDR systems to add up the step vectors: step detection, step length estimation and heading estimation. Step detection can be achieved by detecting the cyclic peaks in acceleration measurements produced by human movement with methods, like peak detection, based on the difference between moving and motionless standing [16,20,21], or methods making use of the periodical pattern like zero crossing detection and autocorrelation [1,22]. For step length estimation, some formulas [23,24,25] have been put forward with reported high accuracy, taking account of acceleration, walking frequency, and other possible factors [26,27]. Heading can be derived from integration of gyroscope, which is the same as the INS scheme.

Manuscript received July 30, 2018. This work was supported by the National Natural Science Foundation of China (No. 61671034).

The authors are with the School of Electronic and Information Engineering, Beihang University, Beijing, 100083, China (e-mail: whdjohnson@gmail.com; congli_bh@buaa.edu.cn; qhlmmm@sina.com).

In addition, magnetometers, which are often included in smartphones, can be utilized to estimate attitude of the device together with accelerometer, as an approach independent from gyroscope. These two independent methods of computing user heading can be integrated together to get better estimations [13,14].

Dead reckoning positioning systems feature high independence from the environment, requiring neither complicated device deployment nor laborious site survey. However, error drifting still remains a serious problem for dead reckoning methods in spite of years of research in this area, especially when low-cost MEMS sensors in smartphones are chosen as measuring tool. Of the three major parts of the PDR approach, error drifting in heading could result in the largest trajectory error. On the other hand, it has been proposed that many corridors inside buildings share the style of straight line, a useful feature for constraints like heuristic drift reduction (HDR) [28,29]. Therefore, in this paper, a pedestrian positioning system is devised to tackle the error-drifting problem with the aid of the straight-line feature in indoor environments. To utilize the straight-line feature, accurate classification of straight-line segments and curve segments in the tracks is required. Sensor measurements like angular velocity are usually employed for the classification task. Meanwhile we can also take advantage of other signals like frequency-modulated (FM) signal to improve the classification result while maintaining sufficient independence from the external environment. Thanks to the fact that wavelength of FM signal, around 3 meters, are comparable to the size of common indoor equipment, FM signal is confronted with much less attenuation while propagating in indoor environment than other high-frequency signals like GNSS and WiFi signals. FM signal characteristics at one position, also known as signal fingerprint in fingerprinting systems [30,31,32] vary across indoor space. Thus different signal variation trend might be detected while walking on different routes. This feature is utilized to integrate FM signal strength measurements and MEMS sensor measurements to classify straight and turning moments.

In this paper, a real-time indoor pedestrian positioning system using MEMS sensors and FM receivers in smartphones is designed to produce accurate pedestrian trajectories by constraining heading error drifting. Data collecting equipment used in this system comprises a three-axis accelerometer, three-axis gyroscope, three-axis magnetometer, and an FM receiver in a smartphone. Random forest algorithm is applied to achieve real-time accurate motion mode detection, the classification of turning and straight line moving, based on integration of FM and sensor signals. Then a measurement reliability selection scheme is employed to filter aberrant magnetic measurements and select the reliable ones, from which final headings of straight-line periods are derived. Detailed experiments are conducted to evaluate the performance of the proposed method. It's illustrated by the experiments that error drifting can be effectively constrained by the proposed system.

The rest of the paper is organized as follows: in Section II the details are described of step detection, step length estimation, motion mode recognition, and heading estimation method. Then performance of the system is analyzed and evaluated by practical field experiment in Section III. Finally conclusions and future works are summarized in Section IV.

II. System Design

A. System Architecture

Overall architecture of the system proposed in this paper is illustrated as Fig. 1. Acceleration signal is used to detect step events and number of steps, in addition with estimation of lengths of each step. Heading is divided into two parts: heading of straight-line periods and heading of turning periods. Classification of turning and straight-line periods is implemented by a random forest classifier with data from inertial sensors and FM receiver. Headings of straight-line periods are estimated with magnetic data only whereas headings of turning periods are estimated with measurements from gyroscope. Finally, trajectory is generated with step number, step lengths, and headings.

B. Coordinate Transformation & Attitude Computation

Direct output of three-axis MEMS sensors are expressed in the Local Coordinate System (LCS) whereas positions and other navigation information are usually given in the Global Coordinate System (GCS). As has been stated in previous literatures [33,34], transformation from GCS to LCS can be achieved by a rotation matrix R:

$$R = \begin{bmatrix} c\gamma c\psi + s\gamma s\theta s\psi & -c\gamma s\psi + s\gamma s\theta c\psi & -s\gamma c\theta \\ c\theta s\psi & c\theta c\psi & s\theta \\ s\gamma c\psi - c\gamma s\theta s\psi & -s\gamma s\psi - c\gamma s\theta c\psi & c\gamma c\theta \end{bmatrix} \quad (1)$$

, where c denotes cos function, s denotes sin function, ψ denotes the yaw angle, θ denotes the pitch angle, and γ is the roll angle. If a vector in LCS needs to be converted to GCS, the corresponding rotation matrix would be the transpose of the R matrix.

In a specific place, we may deem the gravity vector and the magnetic field vector as constant in a short period. Thus, when the device stays static or moves with a constant speed vector, accelerometer and magnetometer directly measure the projections of the gravity vector and magnetic field vector, leaving us the opportunity to attain attitude angles of the device with these two types of sensors as the following equations:

$$\theta = \operatorname{atan2}\frac{a_y}{\sqrt{a_x^2 + a_z^2}} \quad (2a)$$

$$\gamma = \operatorname{atan2}\frac{-a_x}{a_z} \quad (2b)$$

$$\psi = \operatorname{atan2}\frac{m_x\cos\gamma + m_z\sin\gamma}{m_y\cos\theta + m_x\sin\theta\sin\gamma - m_z\sin\theta\sin\gamma} + \delta \quad (2c)$$

, where $[a_x, a_y, a_z]$ is acceleration vector, $[m_x, m_y, m_z]$ is the

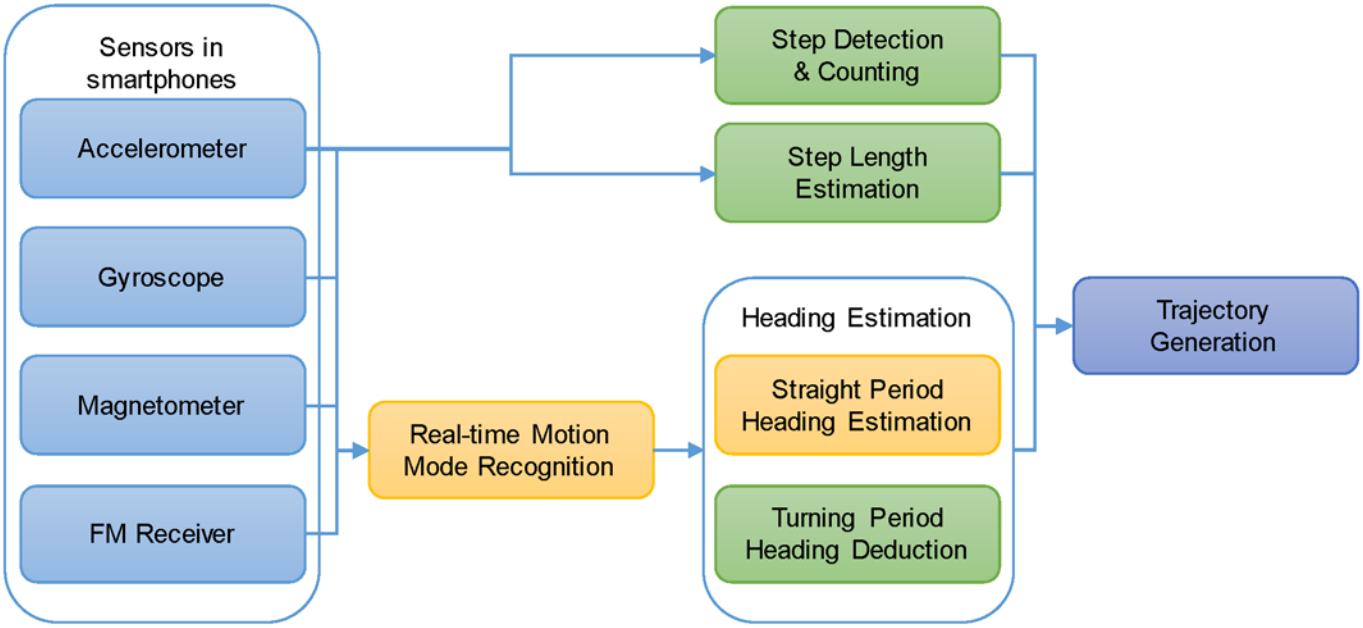

Fig. 1. Overall system architecture.

magnetic field strength vector, and δ is the regional constant magnetic declination.

In this way we can get complete attitude angles of the device with an accelerometer and a magnetometer, although theoretical accuracy is only guaranteed when the device is static or moving with a constant speed, and magnetic interference should be nearly zero. In fact, experiments in this paper are conducted with a mobile phone carried in front of the chest of the test taker. And the experiment taker walks at a normal constant speed without high dynamics. Therefore estimation in this method is reliable to some extent [14]. Moreover, this calculation method is free from cumulative error, an advantage not shared by the method of angular velocity integration.

C. Step Detection & Counting

Step detection is completed with z-axis acceleration data in GCS by a mixed method incorporating zero detection, peak detection, and duration constraint. Acceleration in z-axis of GCS is selected due to its insensitiveness to device posture while exhibiting cyclic oscillation pattern in the walking/running process. Output data from accelerometer are first smoothed with a low-pass filter to remove irregular noise. Then pitch and roll angles are calculated according to equation (2a), (2b), and (2c). With pitch and roll angles, we can rotate LCS two times as described in the previous section, after which positive direction of z axis in LCS and GCS became consistent. After the rotations z-axis value of acceleration is composed of gravity and vertical acceleration of the device. Estimation of the gravity vector is completed by detecting and taking the mean value during a static period. Then the gravity component is removed and device vertical acceleration is extracted.

Types of restrictions exerted on step events in this paper are similar to the method adopted by Qian [27]. The cyclic pattern of human movement produces cyclic peaks in acceleration as illustrated in Fig. 2. Thus acceleration peaks should be detected so as to count steps.

A detected peak of vertical acceleration must first meet the following requirements:

$$a^l_{M-1} \cdot a^l_M \le 0 \quad (3a)$$

$$a^l_N \cdot a^l_{N+1} \le 0 \quad (3b)$$

$$\max(|a^l|) > a^l_{thres} \quad (3c)$$

, where a^l is the vertical acceleration in the navigation frame with gravity component removed, M is the beginning moment of the specific peak, N is the ending moment of the specific peak, a^l_{M-1}, a^l_M, a^l_N, and a^l_{N+1} are the vertical linear acceleration values in the navigation frame at corresponding moments, and a^l_{thres} is the minimal requirement for absolute vertical linear acceleration in the navigation frame.

In this way we can roughly find out the acceleration peaks. Some of the detected peaks might be caused by sensor noise with a feature of very short duration. Whereas some other detected peaks might last too long with values much smaller than the threshold. For these aberrant results, limits on step duration are essential to remove them so that the detection results are reliable. Once a peak with duration shorter than threshold T_{min} is detected, it will be regarded as false alarm and will not be taken as valid result. If a peak is detected with duration longer than threshold T_{max}, moments after duration T_{max} would be regarded as static standing moments.

After the operations above we can get the exact beginning and ending moments of each step. An example of peak and step detection result is shown in Fig. 2, where each peak/step is denoted by a non-zero value and value of neighboring peaks/steps are different in order to distinguish them. To test the accuracy of the step detection algorithm, walking experiment was conducted on a standard 400-meter athletic track. There were totally 20 laps, made up of 13,356 steps, of

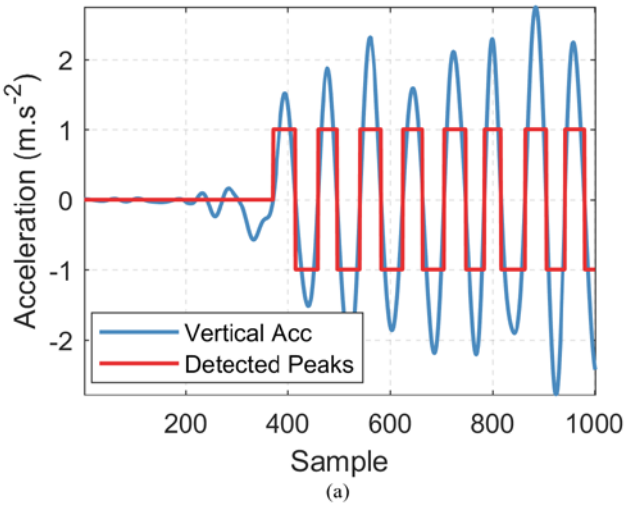

Fig. 2. Part of peak and step detection results. (a) Detection result of acceleration peaks. (b) Detection result of steps.

sensor data collected in 133.5 minutes. Detection result of the proposed algorithm is 13,322 steps, with an accuracy of 99.75%.

D. Step Length Estimation

In the PDR scheme step length is utilized together with heading to attain the position change after one step. The length of each step is related to multiple factors: variation in acceleration, walking frequency, pedestrian height etc. In this paper, the Weinberg approach [23] is adopted to estimate step length. Based on simplification of human walking motion, the Weinberg approach estimates the length of a stride, the process of one step by one leg and a following step by another, as the following equation:

$$d = k \cdot \sqrt[4]{a_{max} - a_{min}} \tag{4}$$

, where d is the length of one stride, k is an empirical constant, a_{max} and a_{min} are the maximal and minimal vertical acceleration value. As stated in [23], step length error of this method can be restricted to no more than $\pm 8\%$.

E. Heading Estimation

Heading estimation is the most difficult part of the PDR algorithm because a tiny error in heading can lead to quite large position error. The two sets of heading estimation methods, one of which integrates angular velocity and the other utilizes accelerometer and magnetometer, both suffer from problems in spite of unique advantages. For the angular integration method, integration result is reliable within short duration yet cumulative error would deteriorate positioning accuracy after long time. As for the method using accelerometer and magnetometer, it is free from error accumulation but vulnerable to magnetic distortion in indoor environment.

Inside buildings many paths like corridors are straight and common human walking route tend to be straight in such paths like corridors. The straight-line feature of indoor paths can be utilized to aid the pedestrian positioning system as the HDR method [28,29]. In this paper the straight line feature is also utilized, but the implementation is different from previous literatures. Heading estimation in this paper is composed of two steps. First a random forest classifier is designed to distinguish straight/turning moments with FM and sensor measurements. Then based on the classification results, true headings of straight periods are extracted from accelerometer and magnetometer outputs.

1) Random Forest Classification

Indoor paths can be segmented into straight and curved parts. Straight/curved segment detection is the basis for separate processing for them. A simple way to discriminate them is to apply a threshold on the absolute value of angular velocity with respect to z-axis in GCS as the following equation:

$$|\omega_z^{GCS}| \geq \Omega_{z,thres} \tag{5}$$

, where ω_z^{GCS} is the angular velocity with respect to z-axis in GCS and $\Omega_{z,thres}$ is the threshold for it. If there is any change in pedestrian heading, a spike of ω_z^{GCS} would appear and the turning would be detected. Although simple and effective for high-precision inertial units, this method might fail when applied to low-cost MEMS gyroscopes due to noise interference. Curves with small curvature might also be hard to detect since change rate of heading could be very low and corresponding spike might be submerged by noise. Another method is to apply a time window to the change rate of heading and compute the total change amount of heading in the time window. To compute the change amount the beginning and ending moments in the window may be utilized as followed:

$$|\psi_n - \psi_{n_0}| \geq \psi_{thres} \tag{6}$$

, where ψ_n and ψ_{n_0} are headings at moment n and moment n_0, ψ_{thres} is the corresponding threshold. Another way is to use the maximum difference of heading in the time window:

$$\max\{|\psi_k - \psi_p|\} \geq \psi_{thres}, \quad k, p = n_0, \cdots, n \tag{7}$$

, where ψ_p and ψ_q are heading at corresponding moments in the time window.

Once the change amount exceeds a threshold, a turning event is detected. However, delay would be introduced by this method, especially for curves with small curvatures where a long time window is needed to make the judgment.

Apart from MEMS sensors, there are some other components in smartphones with measuring function like the WiFi/Bluetooth/FM chip. Of the electromagnetic signals measurable for smartphones, FM signal, for its pervasiveness, can be employed to assist our detection while maintaining high independence of the system. The integration of FM and sensor data is completed by a random forest classifier.

Random forest is a learning method that implements classification/prediction by constructing multiple decision trees and synthesizing outputs of the individual trees. Decision tree is a tree-like structure where each non-leaf node represents one test with respect to one feature, each branch represents one test result and each leaf node represents one class label (for classification) or prediction (for regression). Decision trees are vulnerable to overfitting in spite of simplicity, whereas this defect can be remedied by random forest. For each decision tree in random forest, samples and features used for its training is randomly selected from the general sample and feature set. And then the majority vote of all the trees is taken as the output class label of the random forest. Thanks to the random selection of samples and features, decision trees in random forests are de-correlated and result of the forest is resistant to overfitting.

With determined data source, algorithm, and task goal, we can move to detailed procedures. Direct measurements available from smartphones are the received signal strength (RSSI) of FM radio, device acceleration, angular velocity, and magnetic field strength. Sampling rate of accelerometer, gyroscope and magnetometer are all set to 50 Hz. For the FM receiver chip, it costs about 0.1 second to tune to a new FM frequency and read RSSI, resulting in the actual sampling rate for each FM channel to decrease with the increase in channel number. Therefore, three FM channels are selected for the experiments with considerations on signal strength, stability, and actual sampling rate.

To clearly describe the motion state of one specific moment, we need to extract features from raw input data. An array of 52 dimensions of features as listed below are calculated after a time window is applied to input data stream:

1. RSSI of each FM channel;
2. Standard deviation of RSSI in the time window for each FM channel;
3. RSSI Difference of beginning and ending moment in the time window for each FM channel;
4. Difference of maximum and minimum RSSI in the time window for each FM channel;
5. Energy of RSSI in the time window for each channel;
6. Mean frequency of the spectrum of RSSI in the time window for each channel;
7. Standard deviation of auto correlation array of the RSSI in the time window for each channel;
8. Difference of beginning and ending value of the auto correlation array of the RSSI in the time window for each channel;
9. Difference of maximum and minimum value of the auto correlation array of the RSSI in the time window for each channel;
10. Three-axis acceleration measurement;
11. Three-axis angular velocity measurement;
12. Three-axis magnetic field strength measurement;
13. Standard deviation of three-axis acceleration in the time window;
14. Standard deviation of three-axis angular velocity in the time window;
15. Attitude angles calculated from gyroscope measurements;
16. Attitude angles calculated from accelerometer and magnetometer measurements;
17. Standard deviation of yaw angle calculated from gyroscope measurements (1 dimension);
18. Difference of yaw angles calculated from gyroscope measurements at beginning and ending moments in a time window (1 dimension);
19. Standard deviation of yaw angle calculated from magnetometer measurements (1 dimension);
20. Difference of yaw angles calculated from magnetometer measurements at beginning and ending moment in a time window (1 dimension);

In the feature list above, unless specially noted, each item contains 3 dimensions of features. There are two types of labels in the output set of the classifier: straight line walking moments, when the carrier is walking in a straight line, and turning moments, when the carrier is making a turn. True class labels for training are provided by the aforementioned offline method which monitors total heading change within a time window.

2) Heading Determination

Reliable classification of straight and turning moments paves the way for separate processing of heading. The main idea of heading estimation in this paper is to restrain heading deviation in straight periods based on the assumption that headings of different moments within the same straight period stay the same. For the straight periods, heading of each step is calculated with moments when the headings are not far from the average heading of the moment. For turning periods, headings are calculated by integration of angular velocity, with the beginning moment of current period as the integration starting moment.

To get the heading of one step in the straight period, first moment selection is conducted based on a set of criterions and then weighted average is applied to generate a reliable estimation of the heading of this step. At the selection stage two types of criterions are utilized: heading deviation from average heading of the straight period, and deviation of magnetic field strength vector from average vector of the period. The criterions are listed as followed:

$$\delta\psi_k = \left|\psi_k - \overline{\psi}(n_0, k)\right| < \psi_{thres} \quad (8a)$$

$$\delta v_k = \left\langle \mathbf{M}_k, \overline{\mathbf{M}}(n_0, k) \right\rangle < v_{thres} \quad (8b)$$

, where n_0 is the beginning moment of this straight period, moment k is one moment in the straight period, ψ_k is the device yaw angle at moment k, $\overline{\psi}(n_0, k)$ is the average yaw angle from moment n_0 to moment k, $\delta\psi_k$ is the deviation angle of device yaw from $\overline{\psi}(n_0, k)$ at moment k, ψ_{thres} is the threshold for the yaw angle deviation, $\mathbf{M}_k$ is the magnetic field strength vector at moment k, $\overline{\mathbf{M}}(n_0, k)$ is the average magnetic vector from moment n_0 to moment k, δv_k is the deviation angle of magnetic

vector from $\overline{\mathbf{M}}(n_0, k)$, and v_{thres} is the threshold for angular deviation of magnetic vector from the average vector $\overline{\mathbf{M}}(n_0, k)$. Each of the two criterions would filter out a set of qualified moments. To integrate the two sets, we tested both the intersection and union of them as the result of selection and found in most cases the union of the two sets would produce more accurate trajectories. Consequently union of the two sets is taken as the filtering result.

With moment selection result, we can work out a compound deviation assessment from the true value for each moment:

$$\delta_k = w \cdot \delta\psi_k + (1 - w) \cdot \delta v_k \tag{9}$$

, where δ_k is the compound deviation of moment k and w is the weight of $\delta\psi_k$. Then final heading of moment k is calculated by weight averaging of headings:

$$\psi_k^{final} = \sum_{k=p_0}^{p} \frac{\psi_k}{\delta_k} \Big/ \sum_{k=p_0}^{p} \frac{1}{\delta_k} \tag{10}$$

, where ψ_k^{final} is the final heading of moment k.

Theoretically deviation in heading or magnetic strength vector at one specific moment should be evaluated with true value in the period, whereas practically what we can obtain is measurements with noise and interference. Thus a practical solution is to take the average value of the whole period as substitute for true value. However, future data are not available in the midst of one period, resulting in that average value from the beginning of the specific period to current moment is used as alternative. Such substitution would of course introduce error as cost of real-time processing. With time going on, such error gradually decreases since more and more information about the straight period is collected and mean value of collected data would be increasingly close to average of the whole period. What's more, calculation for heading of one moment might be burdensome for smartphones. A simple way to ease the burden is to only carry out such calculation at the ending moment of each step.

Headings of turning periods may keep changing, leaving much less space for applying constraints. Therefore, headings of turning moments are calculated by integration of angular velocity. Integration in one turning period starts from the beginning moment of that period. Initial attitude is the same as the attitude at the end of last straight period. In this way every time a new turning period is established attitude deduction is restarted and error drifting is reset to zero. Moreover, all the sensor data in last straight period can be devoted to get a better estimation of initial yaw.

F. Trajectory Generation

Commonly in a PDR scheme, trajectory generation is a step-by-step deduction process:

$$\begin{bmatrix} x_k \\ y_k \end{bmatrix} = \begin{bmatrix} x_{k-1} \\ y_{k-1} \end{bmatrix} + l_k \begin{bmatrix} \sin h_k \\ \cos h_k \end{bmatrix} \tag{11}$$

, where x_k and y_k are the distances from the initial location in the direction of x and y axis at step k, x_{k-1} and y_{k-1} are the distances at step $k-1$, l_k is the length of step k, and h_k is the heading of step k. However in our system, modification is made to the trajectory generation method described above so as to fully utilize the assumption that headings of moments in one straight period stay the same. In this paper, position at step k, if in a straight period, is determined by the following equation:

$$\begin{bmatrix} x_k \\ y_k \end{bmatrix} = \begin{bmatrix} x_{k_0-1} \\ y_{k_0-1} \end{bmatrix} + \sum_{p=n_0}^{k} l_p \cdot \begin{bmatrix} \sin h_k \\ \cos h_k \end{bmatrix} \tag{12}$$

, where step n_0 is the first step of this straight period, x_{k_0-1} and y_{k_0-1} are the coordinates of the last step of the previous turning period, or the beginning moment. Positions of steps in turning periods are still deduced with equation (11). As steps in a straight period increases, more sensor data can be gathered and heading estimation error declines gradually, which would significantly reduce trajectory error as described in Section III.

III. Experiments & Result Analysis

A. Experiment Setup

Field experiments have been designed and conducted to evaluate the performance of the PDR system proposed in this paper. Two aspects are involved in the experiments: evaluation of random forest classifier and assessment of trajectory error.

Experiment data are collected using a Xiaomi Redmi 4 smartphone with built-in accelerometer, gyroscope, magnetometer, and FM receiver. Sampling rate of acceleration, angular velocity, and magnetic field strength are all 50 Hz, whereas the average interval for an FM signal strength measurement to update is 0.117 microsecond. The smartphone is carried by the test taker in front of the chest in the process of walking.

B. Random Forest Classification Experiment

1) Classification Performance

Classification of straight and turning moments is the basis for heading optimization in this paper. Due to the incorporation of FM signal, both site and trajectory shape might affect the performance of the classifier. Therefore walking data of different trajectory shape at multiple sites in two buildings have been collected for the train and test of the random forest classifier.

Data for training were collected at 6 different sites inside the first building. Both straight and turning segments are included in the trajectories. At some spacious sites like halls, curves with radius of as large as 6m are included in the trajectories. At other sites like corridors, only sharp turns are included for the sake of space restriction. It took totally 100.3 minutes to collect all the training data.

Three sites are selected to collect test data, the first two of them in the first building and the last in the second building. None of these three sites were used for train data collecting. What's more, there is only one site in the second building, thus no training data come from the second building. Trajectory at the first site is rectangular with a length of 45.4m and a width of 19.0m. Trajectory at the second site is made up of two straight lines with the same length of 23.7m and two curved segments with the same radius of 6.0m. Whereas trajectory at the third site, in a different building, has a shape of alphabet "T" with a length of 167.0m and a width of 50.0m. Total duration

TABLE I
CLASSIFICATION RESULTS OF TEST DATA, WITH FM FEATURES

Actual Motion Mode	Predicted Motion Mode	
	Turning	Straight-line walking
Turning	**88.0%**	12.0%
Straight-line walking	1.9%	**98.1%**

TABLE II
CLASSIFICATION RESULTS OF TEST DATA, WITHOUT FM FEATURES

Actual Motion Mode	Predicted Motion Mode	
	Turning	Straight-line walking
Turning	**83.5%**	16.5%
Straight-line walking	1.2%	**98.8%**

of test data is 47.7 minutes.

Classification results of test data are shown in Table I. The diagonal cells in the table are the correctly classified moments and the off-diagonal cells are the mistakes made. Table I shows that true positive (TP) rate of turning moments is 88.0% and for straight moments TP rate is 98.1%.

To identify the contribution of FM signal in the classification test above, experiment has also been conducted with FM related features removed for both train and test data. Corresponding classification results are presented in Table II. By comparing Table I and Table II we can find that classification accuracy of turning moments can get an improvement of 5.4% with the aid of FM features, whereas the variation in accuracy of straight-line moments is less than 1%. In fact, error cost of turning moments tends to contribute more to final trajectory error than that of straight-line moments. If part of a straight-line period were wrongly recognized as turning period, heading deduction scheme would fall back to angular integration, the result of which is reliable within a short period. However, if part of a turning period were misclassified as straight-line period, heading of each moment in this period would be recognized as the same value, resulting in severe location deviation. On the other hand, there might be slight increase in false negative output for a classifier with the improvement of true negative detection. Consequently the classification accuracy improvement for turning mode presented in Table I and Table II provides support for the contribution of FM signal, which would be further substantiated in later location determination experiment.

2) Real-time Detection

For comparison, we also tested two other turning detection methods. One of them is to apply threshold to absolute value of z-axis angular velocity in GCS. The other is to apply threshold to yaw angle change within a time. The second is an offline approach since delay would be introduced by the time window, especially for low-cost MEMS sensors. The smaller the curvatures of trajectory segments are, the longer time windows are needed, and hence longer delay would be introduced. To highlight the case, we selected a curve segment, as illustrated in Fig. 3, from the trajectory at the second site for demonstration. The sample curve segment, whose radius is 6m, begins with a 90° sharp turn and ends smoothly in the end.

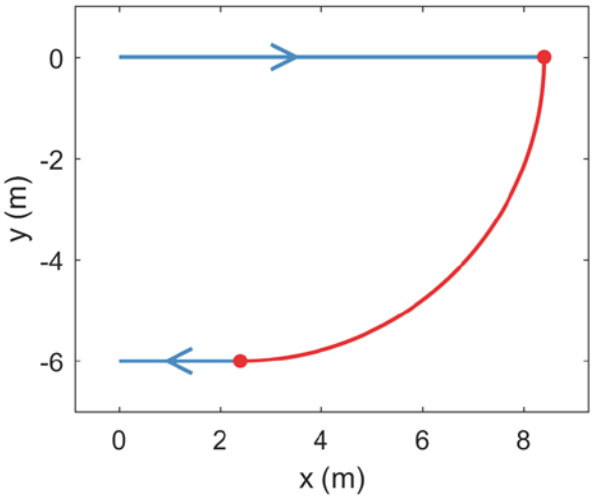

Fig. 3. Sample curve (the red segment) used for turn detection.

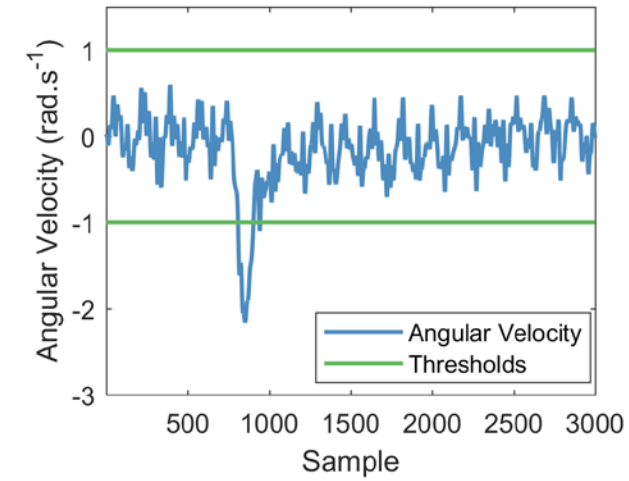

(a)

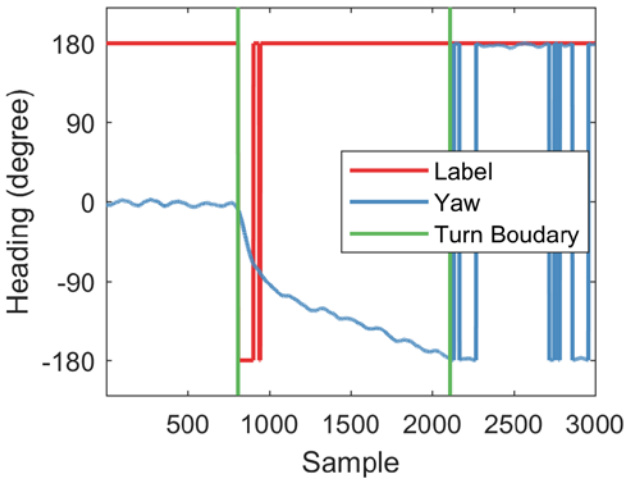

(b)

Fig. 4. Z-axis angular velocity in GCS and corresponding turn detection result. (a) Z-axis angular velocity in GCS. (b) Result of turn detection using z-axis angular velocity in GCS.

TABLE III
MOMENTS OF TAKING PLACE FOR CURVE BEGINNING AND ENDING

Event Type	Gyro Z-axis Approach	Offline Approach (short window)	Offline Approach (long window)	Proposed Approach	Truth
Curve Beginning	810	866	867	810	810
Curve Ending	944	1205	2100	2095	2110

TABLE IV
MOMENTS OF DETECTION FOR CURVE BEGINNING AND ENDING

Event Type	Gyro Z-axis Approach	Offline Approach (short window)	Offline Approach (long window)	Proposed Approach	Truth
Curve Beginning	810	866	867	810	810
Curve Ending	944	1290	2270	2095	2110

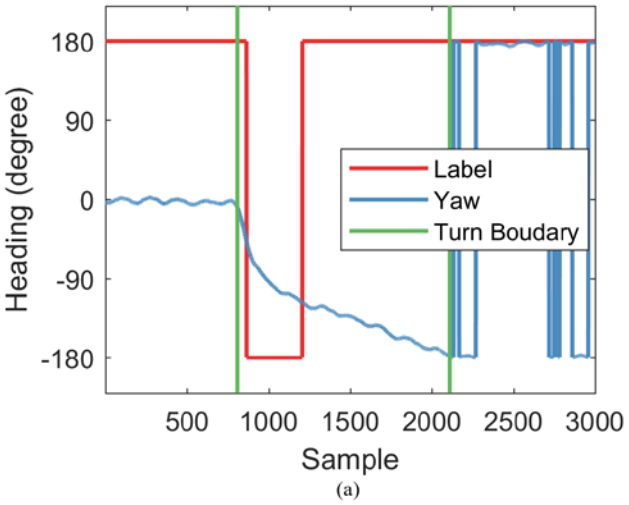

(a)

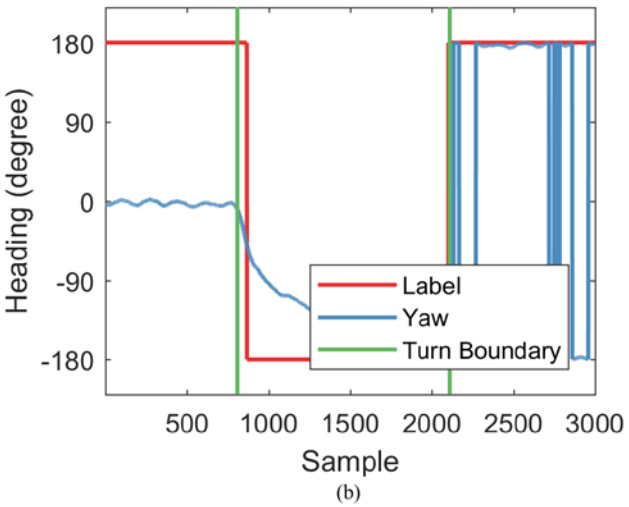

(b)

Fig. 5. Turn detection result of the offline method with different time windows. (a) Duration of the time window is 1 average step; (b) Duration of the time window is 2 average steps.

These two methods and the proposed method are all applied to detect this curve. First a threshold is applied to the z-axis angular rate in GCS. Angular rate in the z-axis in GCS and related detection result is shown in Fig. 4, where the positive label represents straight line walking moments and negative

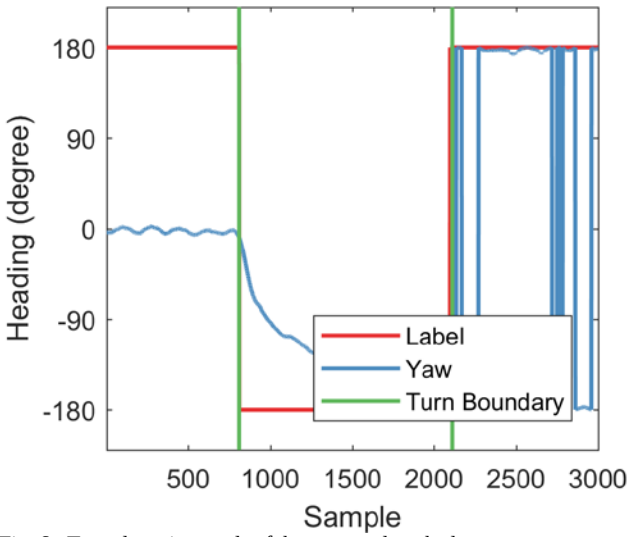

Fig. 6. Turn detection result of the proposed method.

label denotes turning moments. The first moment of the curve is sample 810 and the last moment is sample 2110. As illustrated in Fig. 4, the 90° sharp turn corresponds to the peak in the figure, but at the later smooth turning stage angular velocity has fallen to the level of the straight line stage. This results in the failure of overall detection of this sample curve. The second method is to monitor and apply threshold to yaw angle change in a time window. Detection results of this method are illustrated in Fig. 5, where two time windows with different length are tested for comparison. First a short time window with the duration of one average step is tested. The first subfigure in Fig. 5 shows that only part of the arc segment is detected. As comparison, in the second subfigure the whole arc is successfully detected with a time window of doubled length. For arcs with smaller curvature than the sample arc, longer time window is needed for successful detection, making it difficult to produce reliable detection result within one step. Finally the proposed method is tested, and the turn detection result is illustrated in Fig. 6, where it's shown that the curve is successfully detected. Moreover, moments of taking place and getting detected for curve beginning and ending are listed in Table III and Table IV. It's the delay in the offline method that makes the content of the two tables different. Based on the figures and tables, we can draw the conclusion that the proposed

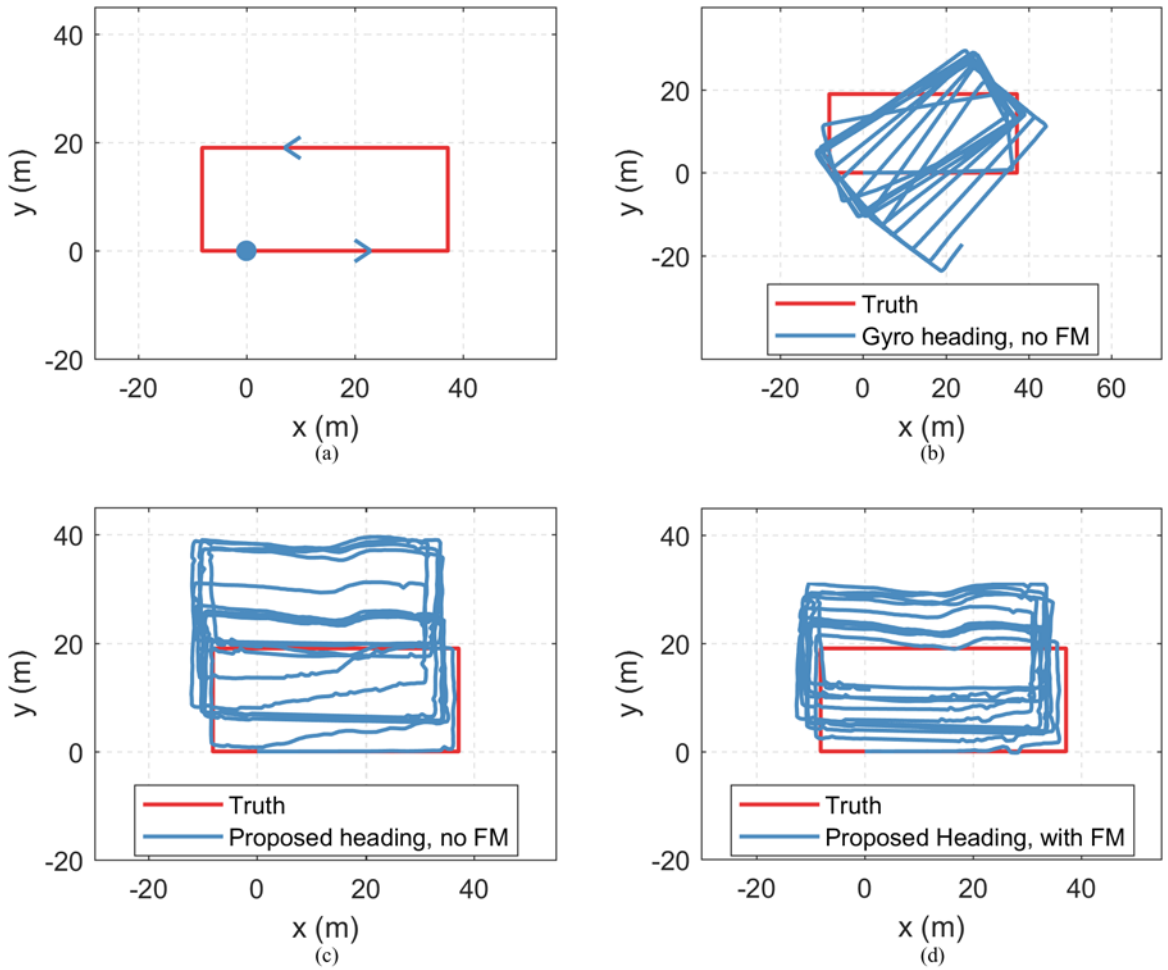

Fig. 7. Comparison of multiple estimated trajectories at the first test site. (a) True trajectory. The blue dot is the beginning and ending position. (b) The first estimated trajectory. (c) The second estimated trajectory. (d) The third estimated trajectory.

approach has achieved successful real-time detection of the whole arc.

C. Location Determination

Positioning performance of the proposed PDR system is evaluated by trajectory generation experiment at the three test sites in the previous classification experiment. At each of the first two sites 10 laps of walking data were collected, whereas at the third site one round-trip is completed on each of the 3 branches of the "T"-shaped route. At each site three types of trajectories are compared, and the differences among them are the method of straight-line constraint and the heading estimation method. A random forest classifier with the entire sensor related features listed in Section II is applied in the generation of both the first and the second trajectory. The difference between them is the heading estimation method. For the first trajectory, headings are attained by angular velocity integration in addition to an averaging operation for headings in straight-line periods. Headings of the second trajectory are computed by the proposed heading estimation method. However, the difference between the second and the third trajectory is the motion mode classifier. The random forest classifier for the third trajectory utilizes not only the sensor related features but also FM related ones.

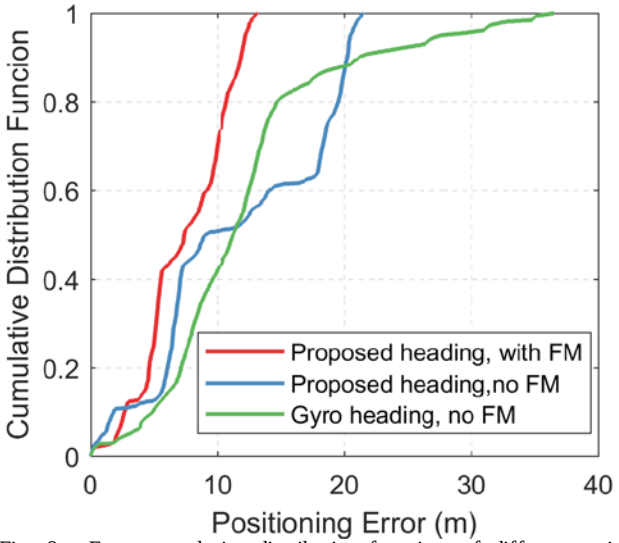

Fig. 8. Error cumulative distribution functions of different estimated trajectories at the first site.

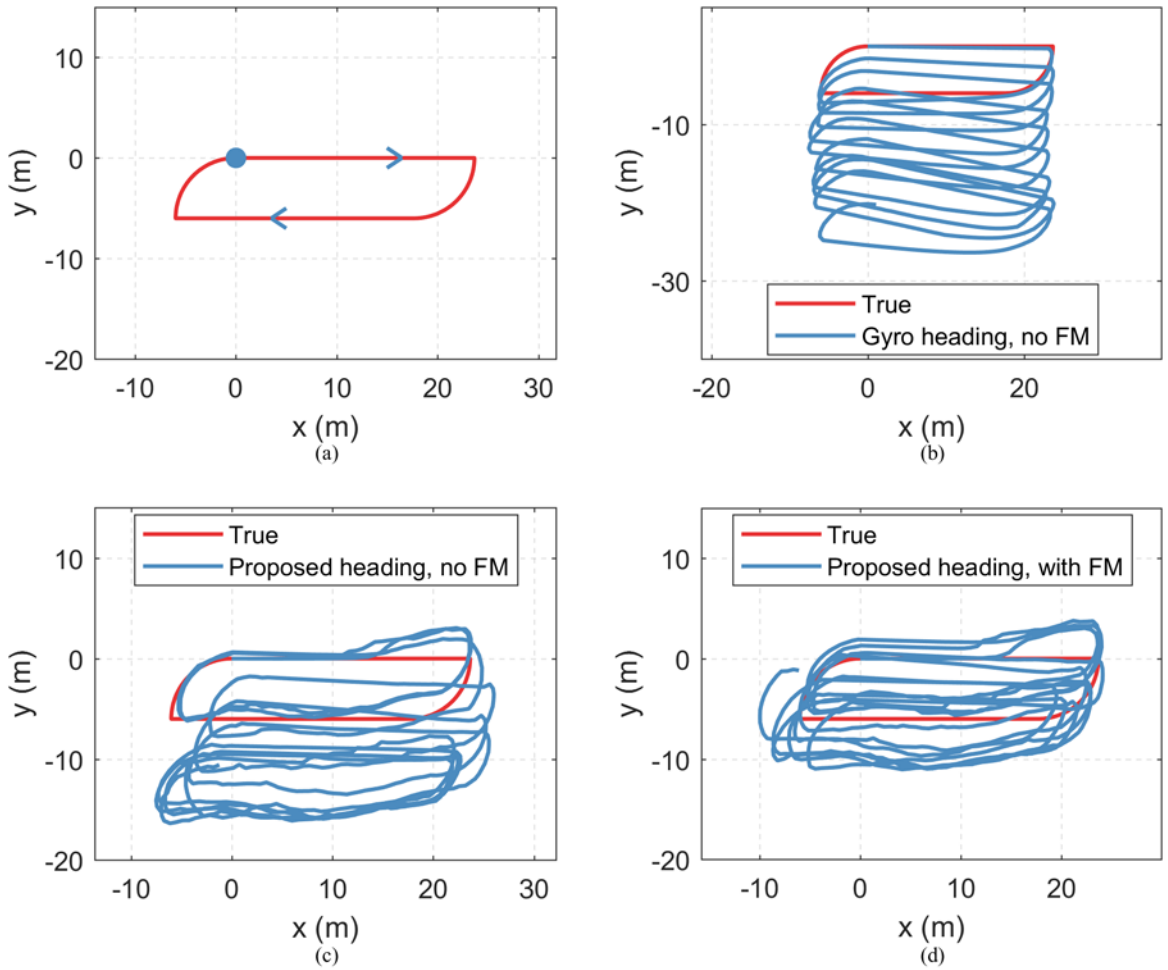

Fig. 9. Comparison of multiple estimated trajectories at the second test site. (a) True trajectory. The blue dot is the beginning and ending position. (b) The first estimated trajectory. (c) The second estimated trajectory. (d) The third estimated trajectory.

For the first site, the true trajectory and three kinds of estimated trajectories are shown in Fig. 7. Trajectory error drifts with all of the three heading calculation methods but the extent of drifting differs. For the first trajectory, error accumulates quickly as turn number increases, resulting in the trajectory to get rotated. For the second trajectory, heading no longer drifts as turn number increases with the aid of the proposed heading estimation method. However, inaccuracy in turning detection causes the disappointing performance of heading estimation in straight-line segments. As for the third trajectory, positioning error is effectively suppressed with precise classification of turning/straight periods and the proposed heading estimation method.

Cumulative distribution functions (CDF) of positioning error for the three estimated trajectories are shown in Fig. 8. From the figure it can be clearly seen that the proposed method outperforms the other two heading computation methods. The largest positioning error of the first trajectory in 10 laps is 36.52m, whereas it is 21.47m for the second trajectory and 13.12m for the third trajectory with the proposed method.

For the second site, the true trajectory and three types of deduced trajectories are shown in Fig. 9. Drifting of angular velocity integration result introduced by multiple turnings leads to severe deviation of the first trajectory, even with the aid of

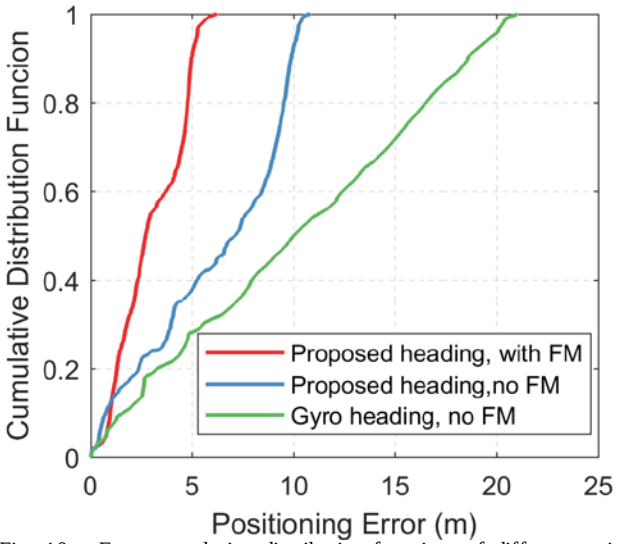

Fig. 10. Error cumulative distribution functions of different estimated trajectories at the second test site.

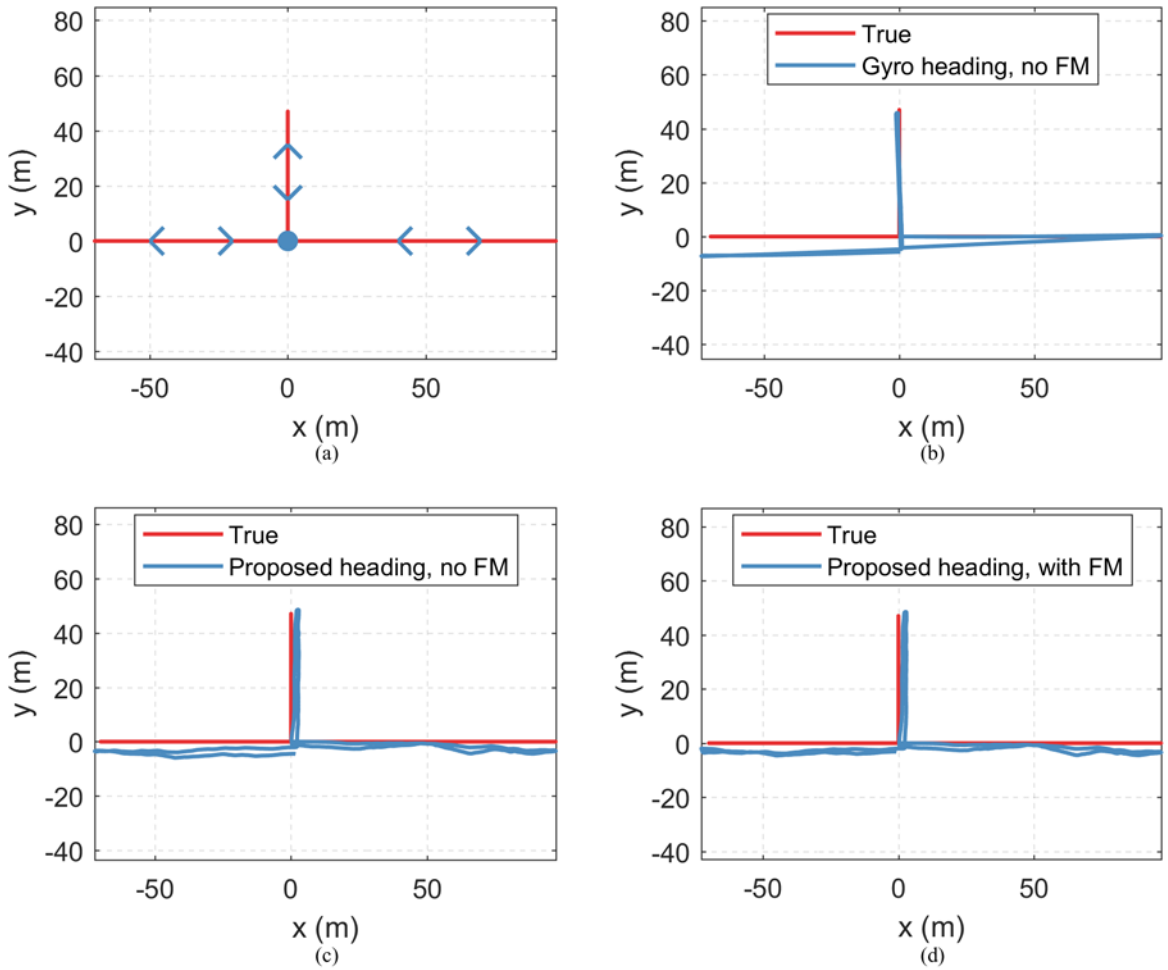

Fig. 11. Comparison of multiple estimated trajectories at the third test site. (a) True trajectory. The blue dot is the beginning and ending position. (b) The first estimated trajectory. (c) The second estimated trajectory. (d) The third estimated trajectory.

straight-line constraint. Position error of the second trajectory, although still drifts away with the climbing up of turning number, is significantly smaller than the first trajectory. As for the third trajectory, with more accurate detection of turning and straight-line moments compared to the second trajectory, error is restrained to the smallest range comparing to the other two trajectories.

CDF figure of trajectory error for the three types of trajectories are shown as Fig. 10. It is illustrated that error of the first trajectory still exceeds that of the other two trajectories. The largest positioning error of the first trajectory is 21.00m, whereas the largest error of the second is 10.82m and for the third it is 6.20m.

Fig. 11 illustrates the true trajectory and three types of estimated trajectories at the third site. First the test taker walks rightward and then turns back to return to the initial position after reaching the right boundary, then walks upward to reach the top boundary before returning, and finally complete the left branch in the same way. Total length of the route is 434.0m. As revealed in Fig. 11, although deviation is restricted in straight periods, drifting induced by turns still drives the trajectory

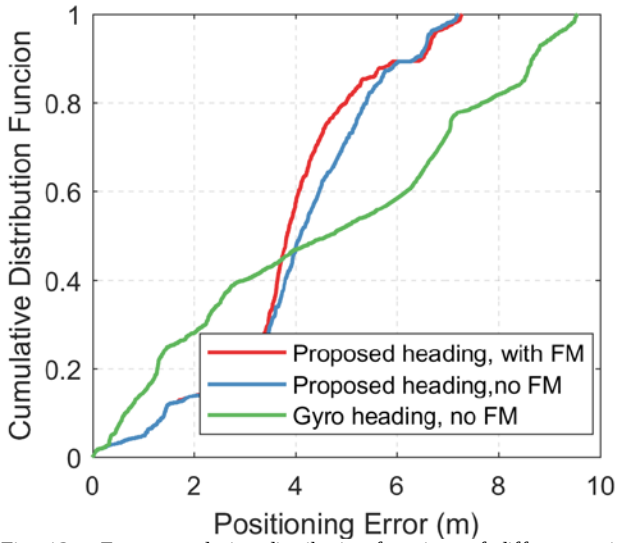

Fig. 12. Error cumulative distribution functions of different estimated trajectories at the third test site.

away. For the second and the third trajectory, the proposed heading estimation method prevents severe drifting.

Errors of the trajectories can be assessed by the CDF curves in Fig. 12, where it is shown that the proposed method outperforms the other two in overall error performance. The maximum error is 9.55m for the first trajectory, whereas it is 7.20m for the second trajectory and 7.26m for the third trajectory. Although the maximum error of the third trajectory is 0.06m larger than that of the second one, overall error of the third trajectory is smaller than the second as the majority of its CDF curve lies to the left of the second's. From these experiment results it can be proved that the proposed PDR system is able to effectively restrain error drifting and yield real-time reliable positioning results.

IV. CONCLUSION

In this paper, a robust real-time indoor pedestrian positioning system is presented using MEMS sensors and FM receiver in smartphones. The proposed system enables us to achieve real-time straight/turning classification with a random forest classifier and extract true headings of straight periods to constrain error drifting induced by heading deviation. Experiments have proved both the classifier and the heading estimation method can improve positioning accuracy, and the combination of them yields the best performance. For future work, we will focus on floor change detection and its integration with current PDR systemto achieve 3D positioning.

REFERENCES

[1] R. Harle, "A survey of indoor inertial positioning systems for pedestrians," *IEEE Commun. Surv. Tuts.*, vol. 15, no. 3, pp. 1281-1293, Apr., 2013.

[2] A. Yazici, U. Yayan, and H. Yücel, "An ultrasonic based indoor positioning system." in *2011 Int. Symp. Innov. Intel. Sys. Appl.*, Istanbul, Turkey, 2011, pp. 585-589.

[3] M. Hazas, and A. Hopper, "Broadband ultrasonic location systems for improved indoor positioning," *IEEE Trans. Mobile Comput.*, vol. 5, no. 5, pp. 536-547, Mar., 2006.

[4] T. Gigl, G. J. Janssen, V. Dizdarevic, K. Witrisal, and Z. Irahhauten, "Analysis of a UWB indoor positioning system based on received signal strength." in *Proc. 2007 4th Workshop Posit., Navigat. Commun.*, Hannover, Germany, 2007, pp. 97-101.

[5] J. Tiemann, F. Schweikowski, and C. Wietfeld, "Design of an UWB indoor-positioning system for UAV navigation in GNSS-denied environments." in *Proc. 2015 Int. Conf. Indoor Posit. Indoor Navigat. (IPIN)*., Banff, AB, Canada, 2015, pp. 1-7.

[6] A. Bekkali, H. Sanson, and M. Matsumoto, "RFID indoor positioning based on probabilistic RFID map and Kalman filtering." in *Proc. 3rd IEEE Int. Conf. Wireless Mobile Comput., Netw. Commun. (WiMob 2007)*, White Plains, NY, USA, 2007, pp. 21-21.

[7] S. S. Saab, and Z. S. Nakad, "A standalone RFID indoor positioning system using passive tags," *IEEE Trans. Indust. Elect.*, vol. 58, no. 5, pp. 1961-1970, May., 2011.

[8] Y. Chen, Q. Yang, J. Yin, and X. Chai, "Power-efficient access-point selection for indoor location estimation," *IEEE Trans. Knowl. Data Eng.*, vol. 18, no. 7, pp. 877-888, Jul., 2006.

[9] S. Eisa, J. Peixoto, F. Meneses, and A. Moreira, "Removing useless APs and fingerprints from WiFi indoor positioning radio maps." in *Proc. Int. Conf. Indoor Posit. Indoor Navigat.*, Montbeliard-Belfort, France, 2013, pp. 1-7.

[10] M. N. Husen, and S. Lee, "Indoor human localization with orientation using WiFi fingerprinting." in *Proc. 8th Int. Conf. Ubiquitous Inf. Manage. Commun.*, Siem Reap, Cambodia, 2014, p. 109.

[11] T.-N. Lin, S.-H. Fang, W.-H. Tseng, C.-W. Lee, and J.-W. Hsieh, "A group-discrimination-based access point selection for WLAN fingerprinting localization," *IEEE Trans. Veh. Tech.*, vol. 63, no. 8, pp. 3967-3976, Oct., 2014.

[12] S. Yiu, M. Dashti, H. Claussen, and F. Perez-Cruz, "Locating user equipments and access points using RSSI fingerprints: A Gaussian process approach." in *2016 IEEE Int. Conf. Commun. (ICC)*, Kuala Lumpur, Malaysia, 2016, pp. 1-6.

[13] Z.-Q. Zhang, X.-L. Meng, and J.-K. Wu, "Quaternion-based Kalman filter with vector selection for accurate orientation tracking," *IEEE Trans. Instrum. Meas.* , vol. 61, no. 10, pp. 2817-2824, Oct., 2012.

[14] X. Yuan, S. Yu, S. Zhang, G. Wang, and S. Liu, "Quaternion-based unscented kalman filter for accurate indoor heading estimation using wearable multi-sensor system," *Sensors*, vol. 15, no. 5, pp. 10872-10890, May, 2015.

[15] P. Strömbäck, J. Rantakokko, S.-L. Wirkander, M. Alexandersson, K. Fors, I. Skog, and P. Händel, "Foot-mounted inertial navigation and cooperative sensor fusion for indoor positioning." in *ION Int. Tech. Meet. (ITM)*, San Diego, CA, US, 2010, pp. 89-98.

[16] L. Fang, P. J. Antsaklis, L. A. Montestruque, M. B. McMickell, M. Lemmon, Y. Sun, H. Fang, I. Koutroulis, M. Haenggi, and M. Xie, "Design of a wireless assisted pedestrian dead reckoning system-the NavMote experience," *IEEE Trans. Instrum. Meas.*, vol. 54, no. 6, pp. 2342-2358, Dec., 2005.

[17] Z.-Q. Zhang, and X. Meng, "Use of an inertial/magnetic sensor module for pedestrian tracking during normal walking," *IEEE Trans. Instrum. Meas.*, vol. 64, no. 3, pp. 776-783, Mar., 2015.

[18] Y. Zhuang, and N. El-Sheimy, "Tightly-coupled integration of WiFi and MEMS sensors on handheld devices for indoor pedestrian navigation," *IEEE Sensors Journal*, vol. 16, no. 1, pp. 224-234, Jan., 2016.

[19] A. R. J. Ruiz, F. S. Granja, J. C. P. Honorato, and J. I. G. Rosas, "Accurate pedestrian indoor navigation by tightly coupling foot-mounted IMU and RFID measurements," *IEEE Trans. Instrum. Meas.*, vol. 61, no. 1, pp. 178-189, Jan., 2012.

[20] B. Krach, and P. Roberston, "Cascaded estimation architecture for integration of foot-mounted inertial sensors." in *Proc. 2008 IEEE/ION Posit., Loc. Navigat. Symp.*, Monterey, CA, USA, 2008, pp. 112-119.

[21] N. Castaneda, and S. Lamy-Perbal, "An improved shoe-mounted inertial navigation system." in *Proc. 2010 Int. Conf. Indoor Posit. Indoor Navigat.*, Zurich, Switzerland, 2010, pp. 1-6.

[22] A. Brajdic, and R. Harle, "Walk detection and step counting on unconstrained smartphones." in *Proc. 2013 ACM Int. Joint Conf. Pervasive Ubiquitous Comput.*, Zurich, Switzerland, 2013, pp. 225-234.

[23] H. Weinberg, "Using the ADXL202 in pedometer and personal navigation applications," *Analog Devices AN-602 Appl. Note*, vol. 2, no. 2, pp. 1-6, 2002.

[24] A. R. Pratama, and R. Hidayat, "Smartphone-based pedestrian dead reckoning as an indoor positioning system." in *Proc. 2012 Int. Conf. Sys. Eng. Tech. (ICSET)*, Bandung, Indonesia, 2012, pp. 1-6.

[25] J. W. Kim, H. J. Jang, D.-H. Hwang, and C. Park, "A step, stride and heading determination for the pedestrian navigation system," *Positioning*, vol. 1, no. 08, pp. 0, 2004.

[26] H. Zhang, W. Yuan, Q. Shen, T. Li, and H. Chang, "A handheld inertial pedestrian navigation system with accurate step modes and device poses recognition," *IEEE Sensors Journal*, vol. 15, no. 3, pp. 1421-1429, Mar., 2015.

[27] J. Qian, L. Pei, J. Ma, R. Ying, and P. Liu, "Vector graph assisted pedestrian dead reckoning using an unconstrained smartphone," *Sensors*, vol. 15, no. 3, pp. 5032-5057, Mar., 2015.

[28] J. Borenstein, L. Ojeda, and S. Kwanmuang, "Heuristic reduction of gyro drift for personnel tracking systems," *The Journal of Navigat.*, vol. 62, no. 1, pp. 41-58, Jan., 2009.

[29] A. R. Jiménez, F. Seco, F. Zampella, J. C. Prieto, and J. Guevara, "Improved heuristic drift elimination with magnetically-aided dominant directions (MiHDE) for pedestrian navigation in complex buildings," *Journal of Loc. Based Serv.*, vol. 6, no. 3, pp. 186-210, Sept., 2012.

[30] A. Popleteev, "Indoor positioning using FM radio signals," Ph.D. dissertation, ICT Int. Doc Sch., Univ. Trento, Trento, Italy, 2011.

[31] Y. Chen, D. Lymberopoulos, J. Liu, and B. Priyantha, "FM-based indoor localization." in *Proc. 10th Int. Conf. Mobile Sys., Appl., Serv.*, Low Wood Bay, Lake District, UK, 2012, pp. 169-182.

[32] V. Moghtadaiee, A. G. Dempster, and S. Lim, "Indoor localization using fm radio signals: A fingerprinting approach." in *Proc. 2011 Int.*

Conf. Indoor Posit. Indoor Navigat., Guimaraes, Portugal, 2011, pp. 1-7.

[33] C. Huang, Z. Liao, and L. Zhao, "Synergism of INS and PDR in self-contained pedestrian tracking with a miniature sensor module," *IEEE Sensors Journal*, vol. 10, no. 8, pp. 1349-1359, Aug., 2010.

[34] W. Kang, and Y. Han, "SmartPDR: Smartphone-based pedestrian dead reckoning for indoor localization," *IEEE Sensors Journal*, vol. 15, no. 5, pp. 2906-2916, May., 2015.

Haidong Wang received the B.S. degree in electronic and information engineering from Beihang University, China, in 2016, where he is currently pursuing the M.S. degree with the School of Electronic and Information Engineering. His research interests include indoor positioning and sensor network.

Li Cong received the M.S. degree from Harbin Engineering University in 2004, and the Ph.D. degree from Beihang University in 2008. She is currently an associate professor in the School of Electronic and Information Engineering, Beihang University. Her research interests include indoor positioning, integrated navigation and tactical navigation.

Honglei Qin received the B.S. degree in computer application from the Changchun Institute of Optical Precision Machinery, Changchun, China, in 1996, and the M.S. degree in electrical engineering from Harbin Institute of Technology, Harbin, China, in 1998, and the Ph.D. degree in navigation, guiding and control from Harbin Engineering University, Harbin, China, in 2001.

He is Leader of the CNT Laboratory of the Electronic Information and Engineering School at Beihang University, China. From July 2001 to May 2003, he worked in Beihang University as postdoctoral researcher. Now he is a full professor with School of Electronic and Information Engineering of Beihang University.

His main research interests comprise Global Navigation Satellite System (GNSS), Radio Navigation System, Integrated Navigation and Opportunity Signal Navigation.